Magnetic actuation of catalytic microparticles for the enhancement of mass transfer rate in a flow reactor

Philip Lisk[1,2], Erell Bonnot[1], Md Taifur Rahman[1], Robert Pollard[2], Robert Bowman[2], Volkan Degirmenci[3], Evgeny V. Rebrov[3,4*]

[1]School of Chemistry and Chemical Engineering, Queen's University Belfast, BT9 5AG, Stranmillis Road, Belfast, UK

[2]Centre for Nanostructured Media, School of Mathematics & Physics, Queen's University Belfast, BT7 1NN, Belfast, UK

[3]University of Warwick, School of Engineering, Coventry, CV4 7AL, UK

[4]Department of Biotechnology and Chemistry, Tver State Technical University, Tver 170026, Russia

*Corresponding author: e.rebrov@warwick.ac.uk

Abstract

The effect of periodic changes in particle velocity on mass transfer to the reacting surface of a magnetic particle with a diameter 225 μm in laminar flow has been investigated in a microfluidic reactor. The periodic particle motion in a fluid was investigated under a sinusoidal magnetic field generated by a quadrupole arrangement of electromagnets around the reactor. The effect of operating frequency of the rotating magnetic field, intensity of the magnetic field, and phase shift between the two sets of magnets on particle dynamics has been studied. Three particle motion modes have been observed depending on the frequency of the applied field. The mass transfer rate was estimated under steady velocity and variable velocity of the particle using a mass transfer correlation by Feng and Michaelides (Int. J. Heat Mass Transfer 44 (2001) 4445). The validity of this correlation for the case of variable particle velocity has been confirmed with a 2D numerical model, describing actual hydrodynamics and mass transfer towards the particle surface. The mass transfer coefficient

depends both on the mean particle velocity and the deviation of velocity from the mean value. The periodic movement with variable particle velocity reduces the mass transfer coefficient by 7.6% as compared to steady state motion with the same mean velocity.

Keywords: Magnetic particle, magnetic actuation, micro reactor, mass transfer.

1. Introduction

Boundary layer flow around a moving surface represents an important type of flow occurring in a number of engineering processes. The applications of moving surfaces include cooling of metal plates on a conveyor belt in a vessel with a cooling fluid, extrusion of polymer plates from a die and heat treatment of materials traveling between a feed roll and wind up roll. The problem has been extensively studied over the last 50 years since the pioneering work of Sakiadis [1, 2] who pointed out the differences in boundary conditions between a moving surface of finite length and a continuous surface. The essential difference between flow with a constant reference velocity and a variable velocity flow is that the particle velocity and thickness of the boundary layer change with time. While various aspects of boundary layer problems with constant reference velocity have been studied [3-5], the effect of non-steady motion of a surface has been explored to a much lesser extent [6-8].

In recent years, hydromagnetic flows and mass transfer have attracted increased research interest due to the exploitation of various magnetic micro and nanostructures. In microfluidics, core-shell catalyst particles can be synthesized consisting of a magnetic core and a catalytic shell. These magnetically controlled particles have been used for cell manipulation, microscopic drug delivery and in microsensor applications [9-11]. Antibody coated magnetic microparticles have also been used in the capture of target species flowing in a 75 μm wide micro channel [12]. Motion of these magnetic particles can be controlled using alternating magnetic fields where the particle velocity depends on the product of the absolute value and gradient of magnetic field. As a result, the particle velocity is not expected to be uniform or constant. Control of particle velocity and trajectory can be adjusted with a feedback control based on video monitoring of the particle location with each time and then correcting the motion by adjustments into the actuation protocol [13, 14]. This procedure is

rather complex and it requires the use of transparent reactor materials which are not always compatible with chemical environment.

In numerous applications in the fine chemical and pharmaceutical industries [15-18], the properties of the final product depends greatly on mass transfer to the catalyst particle surface [19]. Due to the laminar flow conditions prevalent in microchannels, the transport of reactants to the catalyst surface is often limited by diffusion due to the formation of thick hydrodynamic and mass transfer boundary layers around catalytic particles [20]. Application of an external magnetic field by a quadrupole arrangement of electromagnets allows for the controlled manipulation of magnetic particles orthogonal to the direction of flow thus enhancing the mass transfer rates. This, in turn, allows for the use of reactants of higher concentration which leads to process intensification [21].

A quadrupole arrangement of electromagnets is the most common system used for magnetic particle motion control as it allows for a smooth rotational control of the magnetic particles by applying sinusoidal electric signals to two pairs of coils [22] or an oscillating motion by switching two electromagnets on and off [23]. Remote magnetic actuation provides advantages over other methods of energy input in its ability to apply relatively large forces at a distance. It can penetrate through most media, including biological material which is particularly useful for potential applications in microfluidics [24].

Particles move with a variable velocity in a sinusoidal magnetic field due to the magnetic forces at play. For example, when a particle (or an array of individual separated particles) approaches a magnetic pole at maximum field, the magnetic force increases due to the increasing magnetic field gradients and as a result the particle accelerates. As the magnetic field reduces the field gradients reduce and the particle decelerates due to the resistant drag force in the liquid ($F_d = -6\pi\mu RV$). Thus the Re number changes with time

typically in the range between 1 and 50 which in turn which results in varying mass transfer rates in the different sections of reactor.

This problem is analogous to the problem of fluid flow around a stationary isolated sphere at varying Reynolds number. Several authors have considered the latter problem employing experimental, analytical or numerical methods [25, 26]. The problem was solved analytically by using boundary-layer theory along with the concept of similarity solution. The obtained ODE still could present a difficult problem to solve due to the lack of well-defined physical boundary conditions. Brunn and Isemin neglected inertia effects for small particles with diameter below 100 μm at low Peclet (Pe) numbers and derived a correlation for mass transfer from a single rigid spherical particle [27, 28]:

$$Sh = 1 + 0.5Pe + 0.5Pe^2 \ln(Pe) + 0.638Pe^2 + 0.25Pe^3 \ln(Pe) \text{ for Pe} \ll 1 \qquad (1)$$

where $Pe = Re_p\, Sc$, $Re_\mathrm{p} = \frac{\mathrm{v d_p}}{\nu}$, $\mathrm{Sc} = \frac{\nu}{\mathrm{D}}$, v is the relative velocity of the microparticle in the surrounding fluid, ν is the kinematic viscosity of the fluid, $\mathrm{d_p}$ is the particle diameter, and D is the diffusion coefficient.

On the higher end of Pe numbers, Acrivos and Taylor [26] derived a correlation for steady mass transfer from a spherical particle in Stokes flow with small or moderate Reynolds numbers. They provided a correlation for the average Sherwood number (*Sh*), which describes the rate of mass transfer from the sphere.

$$Sh = (0.461\mathrm{Pe}^{-0.33} + 0.6245)\mathrm{Pe}^{0.33} \qquad \mathrm{Pe} > 100 \qquad (2)$$

Magarvey and Bishop [29] revealed that the boundary layer around the sphere remains steady symmetric up to a Re number of 210. Several authors [30-32] have observed that the transition from a steady axisymmetric flow to a steady non-axisymmetric wake flow occurs at a Re number of 211. Below this critical Re number, the exact numerical results obtained for a rigid sphere can be approximated rather well by the following relation [33, 34]:

$$Sh = 0.852\ (ReSc)^{0.33}\ (1 + 0.233\ Re^{0.287} + 1.3 - 0.182Re^{0.355}) \qquad (3)$$

Equation 3 agrees well with the solution proposed by Acrivos and Taylor [26] (Eq.2) for lower range of Re numbers when the flow may be assumed to be steady and axisymmetric.

The current work establishes a theoretical basis for quantifying the contribution from the acceleration and deceleration of particle motion towards mass transfer rate. The effect of the mean particle velocity and the deviation of the mean velocity on mass transfer rate is evaluated using a corresponding numerical model. In the second part of the paper, the actuation protocol for manipulation of a magnetic microparticle is optimised with a view to maximising the rate of mass transfer towards the particle surface where a fast chemical reaction takes place.

2. Experimental

The experiments were carried out in a polydimethylsiloxane (PDMS) flow reactor (diameter: 13 mm, depth: 0.60 mm) located in the centre of a quadrupole set of iron bars (Figure 1). In other words, the reactor can be seen as a cylinder with a height of 0.6 mm (parallel to the gravity vector). The iron bars (length: 14 cm, cross section: 2.5x2.5 cm^2) were connected to four horizontal coils. A reactor was placed over the X-Y stage of an optical microscope (Leica M165 FC) connected to a video camera (Leica DFC310 FX). The coils were coupled in two perpendicular pairs (set A and set B) by two conductive iron bases. The coil pairs were connected to two direct current (DC) power supply units (Kepco BOP 100-2ML). The DC current was controlled in the range from -100 to +100 V with a LabView software.

A sinusoidal actuation protocol was applied to induce an alternating magnetic field inside the flow cell. The sinusoidal functions were defined as: $V_1 = V_0 \sin(\omega t)$ and $V_2 =$

$V_0 \sin(\omega t + \phi)$. The particle velocities and trajectories depended on the applied frequency, phase shift and maximum voltage.

Insert Figure 1 here

Magnetic particles with an average diameter of 225μm were placed in the reactor filled with acetonitrile (Sc number =247). Particle positions were monitored using particle tracing analysis of microreactor images. The images were recorded with a Leica camera at a rate of 20 fps (pixel size of 6.5x6.5 μm^2). The analysis was carried out using an NI-Vision software package producing the x and y pixel positions of the particle as a function of time by detecting dark zones in each image. From these coordinates, the particle position and velocity were calculated. For each actuation protocol (F, ϕ, V_0), the trajectory of the microparticle was monitored over several periods of rotation and then the average velocity and the standard deviation of average velocity were calculated.

3. Mathematical formulation

While a correlation for the mass transfer coefficient has been proposed for a reactive solid particle (Eq. 3) [33], this equation was obtained for stationary flow conditions and therefore it cannot be directly translated to unsteady state flow conditions. Under steady state conditions, the thickness of the boundary layer does not change with time. In the present work, the particle velocity changes with time, therefore the thickness of the velocity boundary layer is also time dependent. In the case of a fast reaction on the particle surface, the thickness of concentration boundary layer also varies with time. To verify the validity of the mass transfer correlation suggested in [33] under hydrodynamic conditions of interest, a

numerical model has been developed. The schematic of the present system and the coordinates are shown in Figure 2.

The numerical model describes the hydrodynamics and mass transfer in case of a fast chemical reaction on the surface of a particle moving with a periodic velocity throughout the reactor. In the flow reactor, particle motion is dictated by a combination of forces, namely the magnetophoretic force due to the magnetic field gradients produced by the magnets, a convective force due to the laminar flow passing through the reactor and the drag force due to the viscous resistance of the fluid. Therefore, the resultant particle velocity is the sum of the particle displacement in the laminar flow and its translation in the time dependent magnetic field. It should be mentioned that under typical experimental conditions the displacement in the laminar flow contributes less than 5% to the total particle velocity and can be omitted.

The numerical model was developed in COMSOL. The depth of the channel perpendicular to the plane of the diagram is assumed to be much larger than the other two dimensions. Hence, the flow can be assumed to be two-dimensional. To simplify the computational procedure, an inverse numerical model was adopted in which the fluid flow was moving around a static circular particle as opposed to the real case of a particle moving throughout the fluid. Actually such situation fully resembles the case where a solid particle is moving in an incompressible fluid flow. However, using a static particle in a periodic fluid flow case significantly simplifies the formulation of the numerical model.

Insert Figure 2 here

The computational domain represents a square region of 0.5 mm x 0.5 mm with a spherical solid particle positioned in the middle (Figure 2). The bottom line (y= –0.25 mm) represents the flow inlet with a periodic velocity in the y-direction and zero velocity in the x-

direction. The top line (y= 0.25 mm) represents the flow outlet with a constant pressure of 1 atm. The left (x= –0.25 mm) and right (x= 0.25 mm) boundaries are symmetry planes. The particle surface ($x^2 + y^2 = r^2$) has a no slip boundary condition.

The hydrodynamics of fluid flow around the fixed particle were governed by the continuity and Navier-Stokes equations for incompressible laminar flow under isothermal conditions (4-6).

$$\frac{\partial v_x}{\partial x} + \frac{\partial v_y}{\partial y} = 0 \tag{4}$$

$$\frac{\partial u_x}{\partial t} + v_x \frac{\partial v_x}{\partial x} + v_y \frac{\partial v_x}{\partial y} = -\frac{1}{\rho}\frac{\partial p}{\partial x} + \frac{\mu}{\rho}\left[\frac{\partial^2 v_x}{\partial x^2} + \frac{\partial^2 v_y}{\partial y^2}\right] \tag{5}$$

$$\frac{\partial v_y}{\partial t} + u_x \frac{\partial v_x}{\partial x} + u_y \frac{\partial v_x}{\partial y} = -\frac{1}{\rho}\frac{\partial p}{\partial y} + \frac{\mu}{\rho}\left[\frac{\partial^2 v_x}{\partial x^2} + \frac{\partial^2 v_y}{\partial y^2}\right] \tag{6}$$

where ρ is the density of the fluid, μ is viscosity of the fluid, v_x and v_y are the components of superficial velocity in the x and y direction, respectively, p is the absolute pressure.

The boundary conditions were as follows:

$$v_y = v(t)|_{t,y=-0.25} \tag{7}$$

$$v_x = 0\ |_{t,y=-0.25} \tag{8}$$

$$v_x = v_y = 0|_{t,x^2+y^2=r^2} \tag{9}$$

$$p = 1\ atm|_{t,y=0.25} \tag{10}$$

$$\frac{\partial p}{\partial y} = 0|_{t,x=-0.25} \tag{11}$$

$$\frac{\partial p}{\partial y} = 0|_{t,x=0.25} \tag{12}$$

Mass transfer is described using a convection and diffusion model with a fast chemical reaction of hydrolysis of benzaldehyde aryl methyl acetal (species A) at the acidic surface of the solid particle:

$$\frac{\partial C_A}{\partial t} + v_x \frac{\partial C_A}{\partial x} + v_y \frac{\partial C_A}{\partial y} = D\left[\frac{\partial^2 C_A}{\partial x^2} + \frac{\partial^2 C_A}{\partial y^2}\right] + R_A \tag{13}$$

where C_A is the concentration of reacting species, D is the molecular diffusivity throughout the domain and R is the reaction rate for an acid catalysed hydrolysis of benzaldehyde aryl methyl acetal.

In the mass transfer model, the bottom line (x= –0.25 mm, see Figure 2) represents a constant concentration boundary condition (Eq. 14). The top line represents a convective flux boundary condition. Similar to the fluid flow domain, the left (y= –0.25 mm) and right (y= 0.25 mm) boundaries are symmetry planes (Eq. 15). A fast catalytic reaction takes places on the particle surface ($x^2 + y^2 = r^2$, Eq. 16).

The following boundary conditions were set for reacting species A

$$\mathrm{C}_A = \mathrm{C}_{A0}|_{t=0,y=-0.25} \tag{14}$$

$$\frac{\partial C_A}{\partial y} = 0|_{t,x=\pm 0.25} \tag{15}$$

$$R_A = \begin{cases} -k_r \mathrm{a}_p \mathrm{C}_A \,|_{t,x^2+y^2=r^2} \\ 0 \qquad\quad |_{t,x^2+y^2\neq r^2} \end{cases} \tag{16}$$

where k_r is the reaction rate constant (29.6 m s^{-1}) [35], C_o is the initial concentration of reacting species A, and a_p is the particle surface area per unit volume.

A free triangular mesh scheme was used throughout the model. Mesh dependency was investigated analysing solutions with decreasing mesh elements. It was found that the maximum and minimum element size required for mesh independence was 1.5 μm in the bulk fluid and 0.01μm in the boundary layer.

The solution was obtained for two velocity components, pressure field and concentration of species A. A transient COMSOL solver was used and solution was converged up to residuals of 1.0×10^{-6} for all components.

4. Results and discussion

4.1 Particle motion in a periodic magnetic field

Particle trajectories at three different frequencies of applied magnetic field are shown in Figure 3a. Particle motion can be assigned to three different forms of cyclic movement shown as modes I, II, and III (Figure 3b). In the frequency range between 0.1 and 0.4 Hz, the particle is pulled towards the nearest magnetic pole by the rotating magnetic field producing circular motion around the outside of microreactor. This motion was very reproducible and will be referred as mode I hereafter. At frequencies of magnetic field between 0.4 and 0.6 Hz, the particle made several rotations near a single pole prior to moving further to the adjacent pole. This type of motion (mode II) was a transition between mode I and mode III, where the particle was oscillating back and forth near a single magnetic pole. This oscillation is due to the particle not having sufficient magnetic response to move along the fast rotating gradients to the neighbouring pole. Mode III was observed at frequencies above 0.6 Hz. In the subsequent discussion, we will mainly consider modes I and II as the particle motion can be described with a simple equation of motion.

Insert Figure 3 here

Due to phase shift (ϕ) between the two sets of coils (Figure 4a), the particle sees a varying magnetic field. This results in a periodic change of the particle velocity between the minimum and maximum values. Figures 4 b and c show the velocities and angular positions determined during the observed circular motion of the particle.

Insert Figure 4 here

Figure 5 shows the effect of magnetic field frequency on particle velocity during a full cycle of field oscillation. The particle experiences intervals of accelerated motion followed

by pauses (Figure 5a). As the frequency increases, the duration of each pause decreases (Figure 5b) and finally a smooth and continuous motion pattern is observed at higher frequencies (Figure 5c).

Insert Figure 5 here

4.2 Mass transfer around a solid particle

In the numerical model described in section 3, the fluid velocity is a periodic function of time

$$v = \bar{v} + b\sin(\omega t) \tag{17}$$

where ω is angular frequency of rotational magnetic field, $\omega = 2\pi F$, F is the frequency of rotational magnetic field, $\bar{v}$ is the average particle velocity and b is the difference between the maximum and average particle velocity. As the chemical reaction occurs solely on the surface of the particle, the concentration of the rate limiting reactant decreases in the boundary layer from the surface concentration to the bulk concentration. The concentration gradient was obtained as a function of angular position around the particle in the range from 0 to 180^{o} at different times corresponding to a single cycle of particle velocity. The four characteristic positions corresponding to the maximum (point A), minimum (point C), and two average velocities (pounds B and D) are shown in Figure 6 and the corresponding concentration profiles for reacting species A are shown in Figure 7.

Insert Figures 6 and 7 here

From these concentration profiles, the local ($k_{f\theta}$) and average (k_f) mass transfer coefficients were obtained by Eqs. 18 and 19, respectively.

$$k_{f\theta} = \frac{D_A \frac{\partial C_A}{\partial r}\Big|_{r=\sqrt{x^2+y^2},\theta}}{C_{A-}C_{SA\theta}} \quad (18)$$

$$k_f = \frac{1}{S}\int_S k_{f\theta} dS \quad (19)$$

where $C_{SA\theta}$ is the surface concentration of species A at an angular coordinate θ, D_A is diffusivity of species A, position $r = \sqrt{x^2 + y^2}$ corresponds to the particle surface and *S* is the surface area in the direction of the flux.

The corresponding local and space averaged Sh numbers were obtained by Eqs. 20 and 21, respectively, at different times corresponding to a single cycle of particle velocity.

$$Sh_{\theta,t} = \frac{k_{f\theta} d_p}{D_A} \quad (20)$$

$$Sh_t = \frac{k_f d_p}{D_A} \quad (21)$$

Finally, time averaged Sh number was calculated by integration of Eq. 22 over one cycle of velocity oscillation (from zero to the time corresponding to point D (t_D) in Figure 6).

$$Sh = \frac{1}{t_D}\int_0^{t_D} Sh_t dt \quad (22)$$

Figure 8a shows the values of the local mass transfer coefficient in terms of Sh number as a function of angular coordinate (θ) at different times within a single cycle of particle motion at a frequency of oscillation of 0.3 Hz (points A-D, Figure 6). As can be seen in Figure 8a, the mass transfer rate remains rather constant in the range of angular positions between 0 and 60^o and then starts to decrease gradually in the downstream direction as the angle increases from 60 to 180^o. The space averaged values over the entire particle surface are shown in Figure 8b as a function of Re number. The dependence of Sh number at a constant velocity case (case 0) is also shown for comparison. As it was discussed in the introduction section, the numerical results obtained for a rigid sphere can be approximated rather well by Eq. 3 which is also presented in Figure 8b. Indeed, a good agreement is observed between the numerical values and Eq. 3 in the entire rage of Re numbers of interest.

The maximum difference between our numerical results and those obtained by Eq.3 does not exceed 20%. The difference can be explained by the fact that we actually used a 2D numerical model instead of 3D analysis performed by Feng and Michaelides [33].

Insert Figure 8 here.

As opposed to a constant velocity case such motion cannot be described with a single hydrodynamic parameter (Re number) as the thickness of hydrodynamic boundary layer changes with time. Therefore, next to the average velocity, an additional parameter should be introduced to characterise particle motion under the oscillating magnetic field. The normalized standard deviation of average velocity (Eq. 23) was chosen in this study as an additional parameter to characterise the time dependent particle velocity.

$$\bar{\sigma}_{\mathrm{v}} = \frac{1}{\bar{v}} \sqrt{\frac{1}{\mathrm{n}} \sum_{\mathrm{i}=1}^{\mathrm{n}} (v_{\mathrm{i}} - \bar{v})^2} \tag{23}$$

A superparamagnetic particle ($\chi > 0$) suspended in a diamagnetic medium is attracted towards a magnetic field. The maximum particle velocity in a weak oscillating magnetic field can be calculated by equalizing the magnetic actuation force (Eq. 24) [36] to the hydrodynamic drag force (Eq. 25): $\mathrm{F}_{mag} = \mathrm{F}_{d}$.

$$\mathrm{F}_{mag} = V_p \frac{\Delta\chi}{2\mu_0} \nabla B^2 \tag{24}$$

$$\mathrm{F}_{d} = -6\pi\eta r_p v_{max} \tag{25}$$

where $\Delta\chi$ is the difference in susceptibility between the particle and the fluid, V_p is the particle volume, μ_0 is the vacuum permeability, and ∇B is the gradient of magnetic flux density, η is the dynamic viscosity of the fluid, r_p is the particle radius, and v_{max} is the maximum velocity of the particle relative to the surrounding fluid. The maximum generated magnetic field of 125 kA m^{-1} corresponds to a particle velocity of 10.8 mm s^{-1}. The minimum

time-averaged particle velocity observed at the minimum gradient of magnetic field (v_{min}) is 1.02 mm s^{-1}.

It is convenient to introduce the dimensionless average velocity ($\tilde{v}$) which is the ratio of the average particle velocity to the highest particle velocity (v_{max}) observed at the specific value of the intensity of magnetic field.

$$\tilde{v} = \frac{\bar{v}}{v_{max}} \tag{26}$$

This parameter can vary from 0.1 to 1.0, the latter extreme value corresponding to the maximum velocity.

Using Eq.3, the corresponding minimum (Sh_{min}) and maximum (Sh_{max}) values of Sh number were found to be 6.23 and 13.94, respectively (Table 2). Figure 9 shows the upper part of the range of possible time-averaged Sh numbers as a function of Re number and σ_v. It can be seen that the minimum value of σ_v observed in this range is 0.08 while the maximum value is 0.65. Following the approach for particle velocity, the standard deviation parameter (Eq. 27) was made non-dimensional by taking the ratio of the standard deviation to its maximum value.

$$\tilde{\sigma}_v = \frac{\bar{\sigma}_v}{\bar{\sigma}_{v,max}} \tag{27}$$

The normalised standard deviation ($\tilde{\sigma}_v$) changes from 0.12 to 1.0, the former value corresponding to motion with the minimum acceleration, and the latter to the case when the particle velocity drops by five times as compared to the average value prior to the next acceleration cycle (see Figure 9).

Insert Figure 9 here.

It can be seen from Figure 9b that in reference case 1 the particle velocity fluctuates between 6.0 and 16 mm s^{-1} while in reference case 2 it changes between 2.0 and 20 mm s^{-1}. In the both cases, the time-averaged Re number calculated over a single period of particle rotation remains the same. However, the time-averaged Sh number (Eq. 28) decreases as compared to the ideal case (Table 2). The higher $\overline{\sigma}_v$ values result in lower values of mass transfer coefficient.

Insert Table 2 here.

$$\overline{\mathrm{Sh}} = \frac{1}{t_1} \int_0^{t_1} (0.852\ (ReSc)^{0.33}\ (1 + 0.233\ Re^{0.287} + 1.3 - 0.182 Re^{0.355}))\mathrm{dt} \qquad (28)$$

As the possible range of values of $\tilde{\sigma}_v$ is limited to a value of 1, it is convenient to introduce a new parameter of $1 - \tilde{\sigma}_v$ that should be maximised to get the highest possible mass transfer rate. The optimised protocol for actuation of magnetic microparticles should provide the maximum of the following objective function (Eq. 29, Figure 7).

$$f = a_1(1 - \tilde{\sigma}_v\ ) + a_2\tilde{\mathrm{v}} \qquad (29)$$

Here coefficients a_1 and a_2 show the effect of the normalised particle velocity and the normalised standard deviation on the mass transfer rate:

$$a_1 = \left.\frac{\partial\, Sh}{\partial \tilde{\sigma}_v}\right|_{\tilde{\mathrm{v}}=const} \qquad (30)$$

$$a_2 = \left.\frac{\partial\, Sh}{\partial \tilde{v}}\right|_{\tilde{\sigma}_v=const} \qquad (31)$$

In other words, these coefficients show the relative change in mass transfer as the $\tilde{\sigma}_v$ changes at constant $\tilde{v}$ and vice versa. It can be seen in Figure 10, that the influence of oscillatory particle behaviour on the mass transfer rate remains rather small as compared to the effect of the average velocity magnitude as a relatively small change in $\tilde{v}$ results in a wider range of possible Sh numbers. The values of a_1= 0.076 and a_2 = 0.924 were obtained from equations 30 and 31 (Figure 10).

Insert Figure 10 here.

It can be seen that the highest time-averaged Sh number and the absolute maximum of objective function *f* would be achieved in case $\tilde{v}$ = 1 and $\tilde{\sigma}_v$ = 0. However, such a case cannot be realised in practice due to the presence of the time dependent magnetic force which is responsible for the particle acceleration during its approach to the magnetic pole and a deceleration period shortly afterwards. The shortest approach to the maximum value is shown in Figure 10 with a solid line (design line). Therefore, in the following experiments the design parameters have been changed in such a way that those values of the objective function are centred along the design line. The effect of magnetic field frequency and amplitude and the phase shift on the normalised average particle velocity and normalised velocity deviation have been studied in a series of experiments where one of these parameters was systematically changed while the other two remained constant. For each individual experiment, the values of objective function *f* were calculated.

Figure 11a shows the effect of operating voltage and phase shift, while Figure 11b shows the effect of the frequency and phase shift. The maximum of objective function is reached at the maximum operating frequency of 0.6 Hz, maximum voltage of 100 V and a phase shift of 90^o.

Insert Figure 11 here.

5. Conclusions

Periodic velocity patterns of a single microparticle with a diameter of 225 μm have been observed in a rotating magnetic field generated by two pairs of electromagnets. Due to the symmetric orientation of the magnetic poles, three modes of particle motion have been observed corresponding to the frequency range of 0.1-0.4, 0.4-0.6 and 0.6-1.0 Hz. Due to non-steady velocity profile, the mass transfer coefficient towards the reacting surface depends on both the time-averaged Re number and its normalised standard deviation. The sensitivity coefficients were estimated for both parameters and it was found that the contribution of the average velocity is more important as compared to the contribution of the periodic acceleration/deceleration due to time dependent magnetic field. The absolute value of particle velocity contributes by 92.4% towards the mass transfer while the effect of the deviation is relatively small and accounts for 7.6%. In other words, the periodic movement with variable particle velocity could reduce the mass transfer coefficient up to 7.6% as compared to steady state motion with the same mean velocity. Based on this information, the actuation protocol was optimized by adjusting the operating frequency and phase shift between two sets of coils to obtain the maximum possible velocity with a minimum standard deviation. The optimised protocol requires a phase shift of 90^{o} and a frequency of 0.6 Hz.

The corresponding mass transfer coefficient can be estimated with an accuracy of 20% taking the time averaged value of Sh number calculated from the Feng and Michaelides [33] correlation for a spherical particle in laminar flow. At low frequencies of the rotating magnetic field, both velocity and concentration boundary layers have enough time to readjust to the new hydrodynamic conditions. Therefore, the correlation derived for steady state conditions can be directly translated to the periodic motion conditions.

Acknowledgements

The financial support provided by the European Research Council (ERC, project 279867), and Russian Science Foundation (project 15-13-20015) is gratefully acknowledged.

Nomenclature

a_1	sensitivity coefficient for mass transfer rate with respect to normalised standard deviation from the average velocity
a_2	sensitivity coefficient for mass transfer rate with respect to average velocity
a_p	particle surface area per unit volume
b	difference between the maximum and average particle velocity
∇B	magnetic flux density
C_A	concentration of benzaldehyde aryl methyl acetal (species A)
C_o	initial concentration of benzaldehyde aryl methyl acetal
D_A	molecular diffusivity of benzaldehyde aryl methyl acetal
d_p	particle diameter
F	rotation frequency of external magnetic field
$k_{f\theta}$	local mass transfer coefficient
k_f	average mass transfer coefficient
k_r	reaction rate constant
n	number of measurement point
p	pressure
r	radius (in polar coordinates)
R	reaction rate
Re_p	Reynolds number
S	surface area in the direction of the flux of species A
Sc	Schmidt number
$Sh_{\theta,t}$	local Sherwood number
Sh_t	space-averaged Sherwood number for the whole particle surface

Sh time-averaged Sherwood number for a single period of velocity oscillation

t time

t_D period of velocity oscillation

v particle velocity

v_x x component of the particle velocity

v_y y component of the particle velocity

V voltage on the coils

V_0 maximum voltage on the coils

V_p particle volume

$\bar{v}$ average particle velocity

$\tilde{v}$ normalised average particle velocity

$v_{\max}$ maximum particle velocity

Greek letters

δ boundary layer thickness

θ angle (in polar coordinates)

μ fluid viscosity

μ_0 vacuum permeability

ν kinematic fluid viscosity

ρ fluid density

$\Delta\chi$ difference in magnetic susceptibility between the particle and the fluid

$\overline{\sigma}_v$ standard deviation from average velocity

$\sigma_{v,\max}$ maximum standard deviation

$\tilde{\sigma}_v$ normalised standard deviation from the average velocity

ϕ phase shift of external magnetic field

ω angular frequency of external magnetic field, ω=2πF

Figure captions

Figure 1. Schematic of the magnetic actuation system showing electromagnets A1-A2 and B1-B2 surrounding the reactor.

Figure 2. Computational domain in the numerical model representing periodic fluid flow around a solid particle. All dimensions are given in mm.

Figure 3. (a) Particle positions under an applied field for frequencies: 0.2, 0.4 and 0.6 Hz. The red line shows to the outer reactor wall. (b) Particle trajectories in the three modes of particle motion. The actual movies corresponding to each motion mode are available in Supplementary Material.

Figure 4. Time dependencies of (a) applied voltage on the two pairs of electromagnets, (b) particle velocity and (c) particle angular position and total distance travelled.

Figure 5. Particle velocity as a function of time for one cycle at three frequencies of rotating magnetic field: (a) $F = 0.2$ Hz, (b) $F = 0.4$ Hz, and (c) F =0.6 Hz.

Figure 6. Particle velocity in two modes of particle motion: constant velocity (case 0) and periodic velocity (case 1). The individual positions representing the concentration gradients in Figure 7 are designated with points A, B, C, and D.

Figure 7. (a) Concentration profile near the reacting particle surface corresponding to point A of a single periodic cycle (see Figure 6). (b-e) Magnified views of

concentration profiles near the reacting particle surface in the range of angular positions between 90 and 180^{o} at different times within a single periodic cycle (points A, B, C and D, respectively, see Figure 6).

Figure 8. (a) Local Sh number as a function of angular position for a periodic particle motion (case 1, Figure 6) obtained at four different times designated with points A, B, C, and D. (b) Average Sh number as a function of mean particle velocity for a constant particle motion (case 0, Figure 6); periodic particle motion (case 1, Figure 6). Sh number correlation [33] is given for comparison.

Figure 9. (a) Calculated Sherwood number as a function of Re number and normalised standard deviation of velocity; (b) particle velocity and corresponding Sh number as a function of time for periodic particle motion with minimum standard deviation (case 1); periodic particle motion with maximum standard deviation (case 2) and constant particle motion (case 0).

Figure 10. Effect of normalised mean particle velocity and normalised mean standard deviation of particle velocity on value of objective function f.

Figure 11. The values of objective function f as a function of different combinations of design parameters: (a) voltage amplitude and phase shift at a constant frequency of oscillating magnetic field, (b) frequency of oscillating magnetic field and phase shift at constant voltage amplitude of magnetic field.

Tables

Table 1. Time-averaged and maximum velocity and the corresponding Reynolds and Sherwood number for different types of circular motion

Case	$\bar{v}$ (mm·s^{-1})	v_{max} (mm·s^{-1})	$\bar{\sigma}_v$	$\overline{Re}$	$\overline{Sh}$
0	10.8	10.8	0.00	5.56	14.0
1	10.8	15.7	0.33	5.56	13.8
2	10.8	19.8	0.60	5.56	13.3

Table 2. Time-averaged values for the minimum and maximum velocity and the corresponding Reynolds and Sherwood number for different types of circular motion

	Minimum	Maximum
$\bar{v}$ (mm·s^{-1})	1.02	10.8
$\tilde{v}$ (-)	0.08	1.0
$\tilde{\sigma}_v$ [a] (-)	0.12	1.0
$\overline{Re}$ (-)	0.51	5.56
$\overline{Sh}$ [b] (-)	6.21	13.94

[a] observed at $\bar{v} = 10.8$ mm·s^{-1}

[b] calculated by Eq. 28

References

[1] B.C. Sakiadis, Boundary-layer behavior on continuous solid surfaces: I. Boundary-layer equations for two-dimensional and axisymmetric flow, AIChE Journal 7 (1961) 26-28.
[2] B.C. Sakiadis, Boundary-layer behavior on continuous solid surfaces: II. The boundary layer on a continuous flat surface, AIChE Journal 7 (1961) 221-225.
[3] F.K. Tsou, E.M. Sparrow, R.J. Goldstein, Flow and heat transfer in the boundary layer on a continuous moving surface, International Journal of Heat and Mass Transfer 10 (1967) 219-235.
[4] V.M. Soundalgekar, T.V. Ramana Murty, Heat transfer in flow past a continuous moving plate with variable temperature, Wärme- und Stoffübertragung 14 (1980) 91-93.
[5] M. Ali, F. Al-Yousef, Laminar mixed convection from a continuously moving vertical surface with suction or injection, Heat and Mass Transfer 33 (1998) 301-306.
[6] E. Magyari, M.E. Ali, B. Keller, Heat and mass transfer characteristics of the self-similar boundary-layer flows induced by continuous surfaces stretched with rapidly decreasing velocities, Heat and Mass Transfer 38 (2001) 65-74.
[7] A.M. Salem, M. Abd El-Aziz, Effect of Hall currents and chemical reaction on hydromagnetic flow of a stretching vertical surface with internal heat generation/absorption, Applied Mathematical Modelling 32 (2008) 1236-1254.
[8] J. Vleggaar, Laminar boundary-layer behaviour on continuous, accelerating surfaces, Chemical Engineering Science 32 (1977) 1517-1525.
[9] M.A.M. Gijs, Magnetic bead handling on-chip: New opportunities for analytical applications, Microfluidics and Nanofluidics 1 (2004) 22-40.
[10] M.A.M. Gijs, F. Lacharme, U. Lehmann, Microfluidic applications of magnetic particles for biological analysis and catalysis, Chemical Reviews 110 (2010) 1518-1563.
[11] I.M. Hsing, Y. Xu, W. Zhao, Micro- and nano- magnetic particles for applications in biosensing, Electroanalysis 19 (2007) 755-768.
[12] S. Van Pelt, R. Derks, M. Matteucci, M.F. Hansen, A. Dietzel, Flow-orthogonal bead oscillation in a microfluidic chip with a magnetic anisotropic flux-guide array, Biomedical Microdevices 13 (2011) 353-359.
[13] M.D. Armani, S.V. Chaudhary, R. Probst, B. Shapiro, Using feedback control of microflows to independently steer multiple particles, Journal of Microelectromechanical Systems 15 (2006) 945-956.
[14] R. Probst, J. Lin, A. Komaee, A. Nacev, Z. Cummins, B. Shapiro, Planar steering of a single ferrofluid drop by optimal minimum power dynamic feedback control of four electromagnets at a distance, Journal of Magnetism and Magnetic Materials 323 (2011) 885-896.
[15] R. Jevtic, P.A. Ramachandran, M.P. Dudukovic, Capillary reactor for cyclohexane oxidation with oxygen, Chemical Engineering Research and Design 88 (2010) 255-262.
[16] L.N. Protasova, E.V. Rebrov, H.E. Skelton, A.E.H. Wheatley, J.C. Schouten, A kinetic study of the liquid-phase hydrogenation of citral on Au/TiO2 and Pt–Sn/TiO2 thin films in capillary microreactors, Applied Catalysis A: General 399 (2011) 12-21.
[17] S. Marre, Y. Roig, C. Aymonier, Supercritical microfluidics: Opportunities in flow-through chemistry and materials science, The Journal of Supercritical Fluids 66 (2012) 251-264.
[18] X. Liu, B. Unal, K.F. Jensen, Heterogeneous catalysis with continuous flow microreactors, Catalysis Science & Technology 2 (2012) 2134-2138.
[19] K. Jähnisch, V. Hessel, H. Löwe, M. Baerns, Chemistry in Microstructured Reactors, Angewandte Chemie International Edition 43 (2004) 406-446.
[20] A.-L. Dessimoz, L. Cavin, A. Renken, L. Kiwi-Minsker, Liquid–liquid two-phase flow patterns and mass transfer characteristics in rectangular glass microreactors, Chemical Engineering Science 63 (2008) 4035-4044.
[21] S.C. Stouten, T. Noël, Q. Wang, V. Hessel, A View Through Novel Process Windows, Australian Journal of Chemistry 66 (2013) 121-130.

[22] S. Melle, O.G. Calderon, M.A. Rubio, G.G. Fuller, Rotational dynamics in dipolar colloidal suspensions: video microscopy experiments and simulations results, Journal of Non-Newtonian Fluid Mechanics 102 (2002) 135-148.
[23] Y. Wang, J. Zhe, B.T.F. Chung, P. Dutta, A rapid magnetic particle driven micromixer, Microfluidics and Nanofluidics 4 (2008) 375-389.
[24] E. Diller, S. Miyashita, M. Sitti, Remotely addressable magnetic composite micropumps, RSC Advances 2 (2012) 3850-3856.
[25] S. Aktar, M. Ruma, M. Alim, Conjugate effects of heat and mass transfer on natural convection flow along an isothermal sphere with radiation heat loss, Open Journal of Fluid Dynamics 3 (2013) 86-94.
[26] A. Acrivos, T.D. Taylor, Heat and Mass Transfer from Single Spheres in Stokes Flow, Physics of Fluids 5 (1962) 387-394.
[27] P.O. Brunn, Heat or mass transfer from single spheres in a low reynolds number flow, International Journal of Engineering Science 20 (1982) 817-822.
[28] P.O. Brunn, D. Isemin, Dimensionless heat-mass transfer coefficients for forced convection around a sphere: a general low Reynolds number correlation, International Journal of Heat and Mass Transfer 27 (1984) 2339-2345.
[29] R.H. Magarvey, R.L. Bishop, Transition Ranges for Three-Dimensional Wakes, Canadian Journal of Physics 39 (1961) 1418-1422.
[30] T.A. Johnson, V.C. Patel, Flow past a sphere up to a Reynolds number of 300, Journal of Fluid Mechanics 378 (1999) 19-70.
[31] A.G. Tomboulides, S.A. Orszag, Numerical investigation of transitional and weak turbulent flow past a sphere, Journal of Fluid Mechanics 416 (2000) 45-73.
[32] M.C. Thompson, T. Leweke, M. Provansal, Kinematics and Dynamics of Shpere Wake Transition, Journal of Fluids and Structures 15 (2001) 575-585.
[33] Z.-G. Feng, E.E. Michaelides, Heat and mass transfer coefficients of viscous spheres, International Journal of Heat and Mass Transfer 44 (2001) 4445-4454.
[34] S. Bhattacharyya, A. Singh, Mixed convection from an isolated spherical particle, International Journal of Heat and Mass Transfer 51 (2008) 1034-1048.
[35] B. Capon, K. Nimmo, General acid catalysed hydrolysis of benzaldehyde aryl methyl acetals, Journal of the Chemical Society, Perkin Transactions 2 (1975) 1113-1118.
[36] S. Bronzeau, N. Pamme, Simultaneous bioassays in a microfluidic channel on plugs of different magnetic particles, Analytica Chimica Acta 609 (2008) 105-112.

Figure

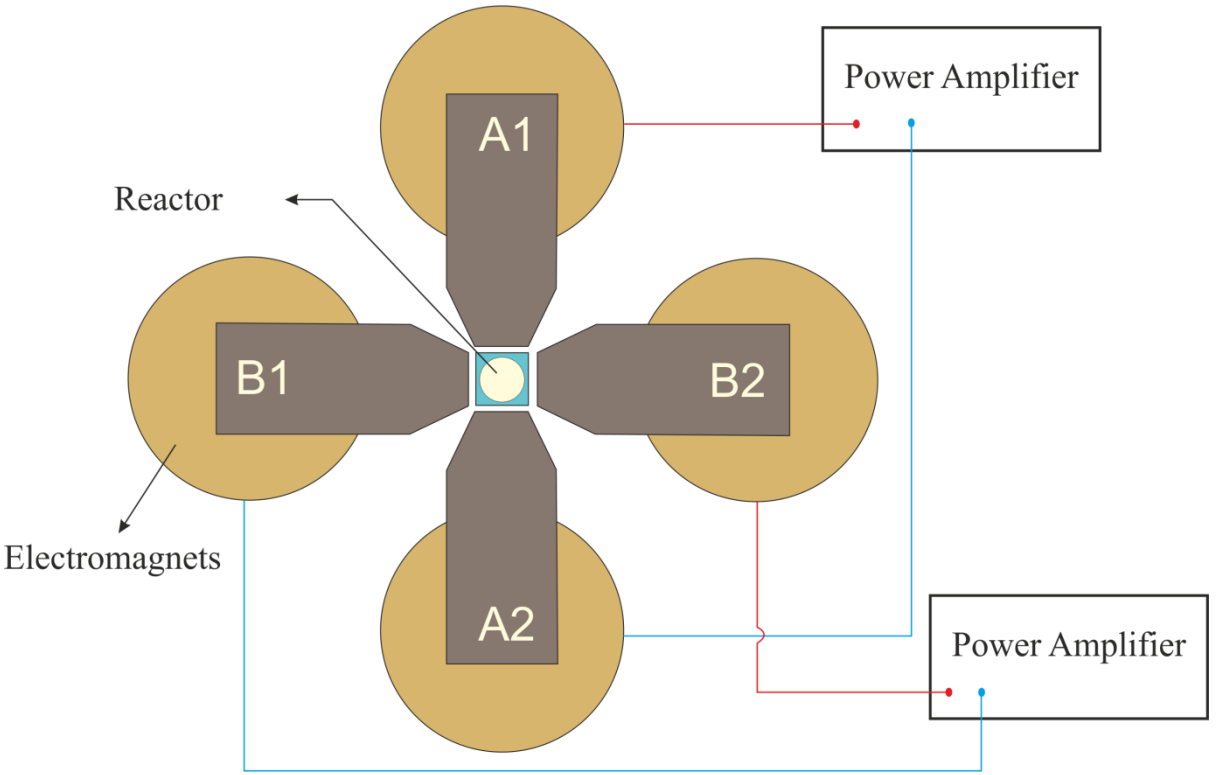

Figure 1

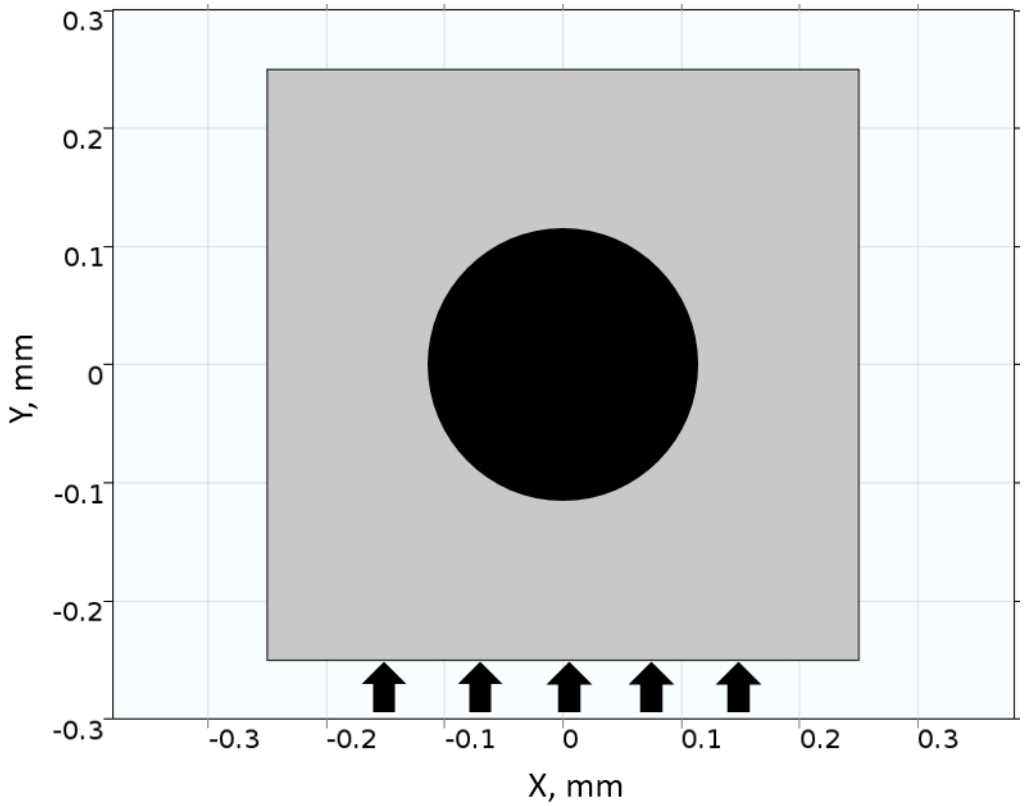

Figure 2

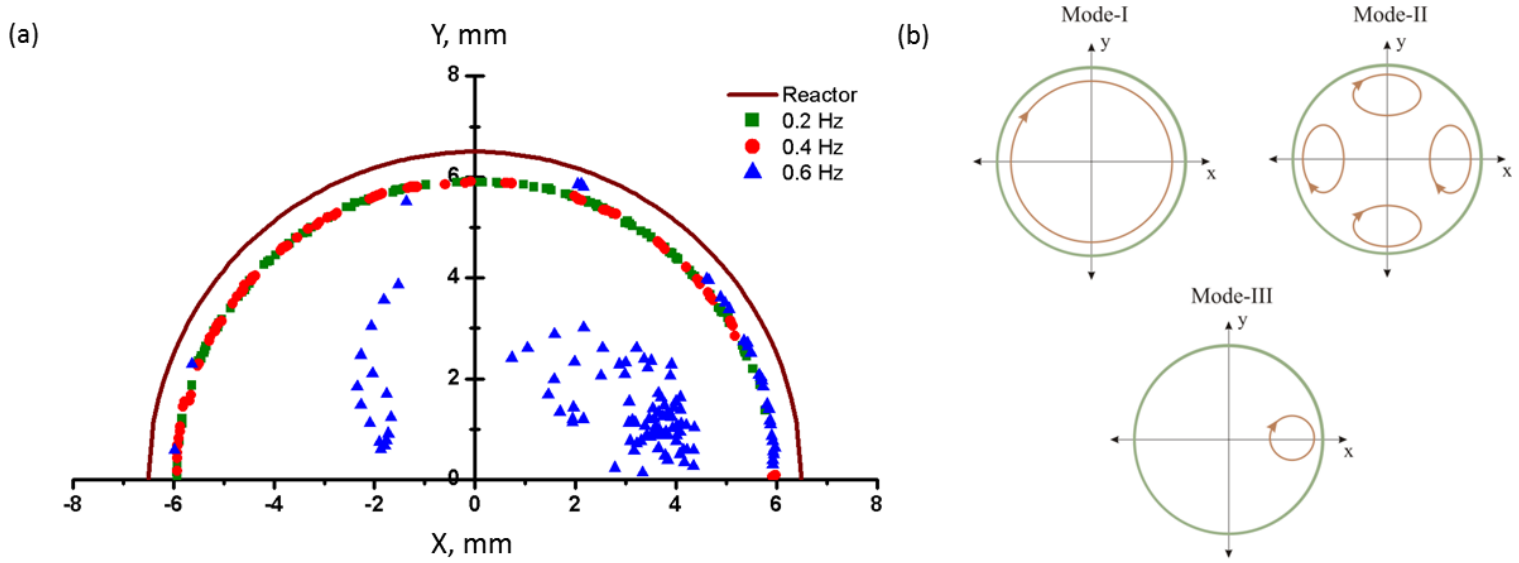

Figure 3

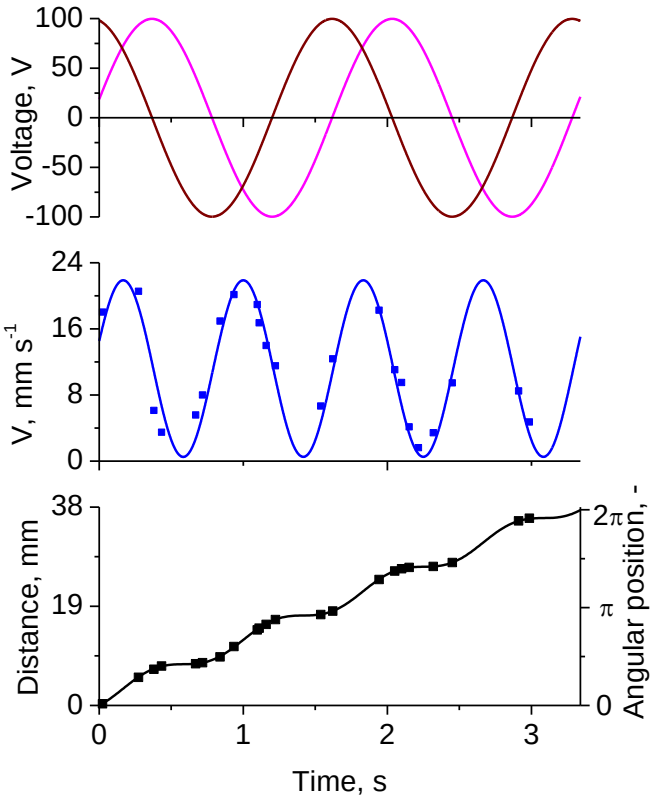
100
50
0
-50
-100
Voltage, V
24
16
8
0
V, mm s-1
38
19
0
Distance, mm
2π
π
0
Angular position, -
0
1
2
3
Time, s

Figure 4

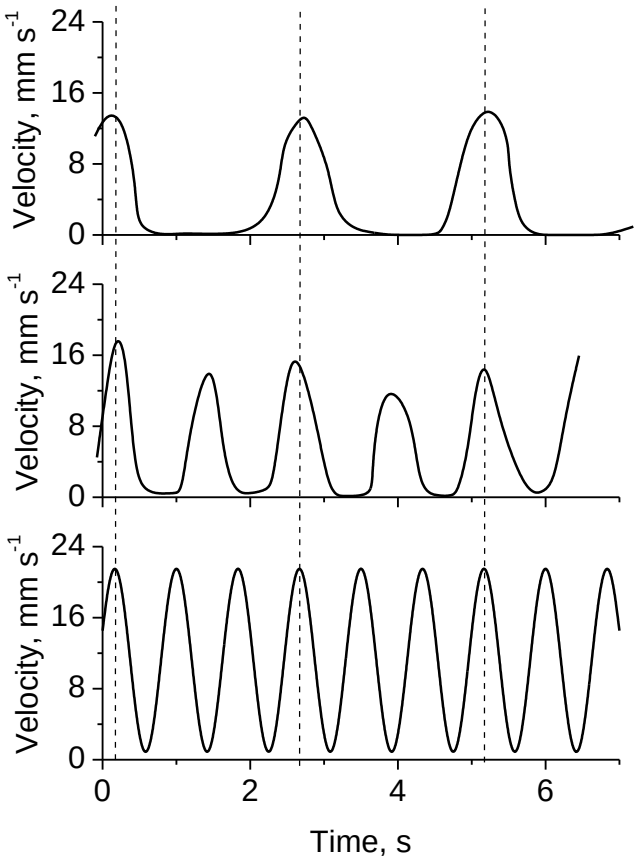
Velocity, mm s-1
24
16
8
0
Velocity, mm s-1
24
16
8
0
Velocity, mm s-1
24
16
8
0
0
2
4
6
Time, s

Figure 5

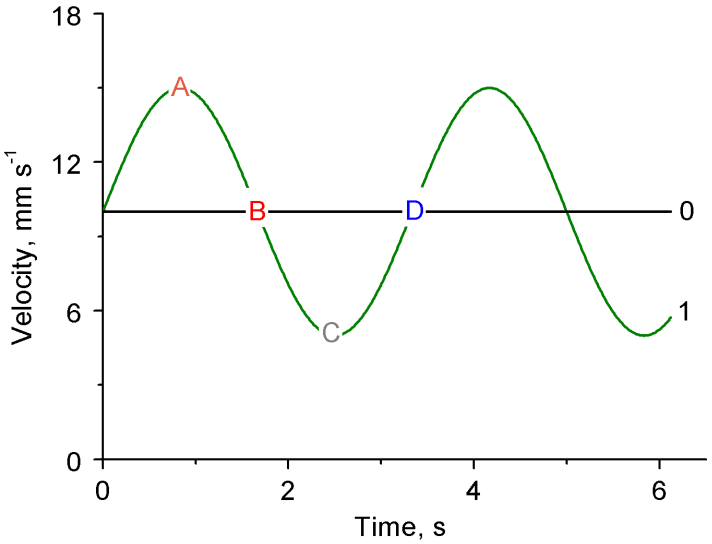

Figure 6

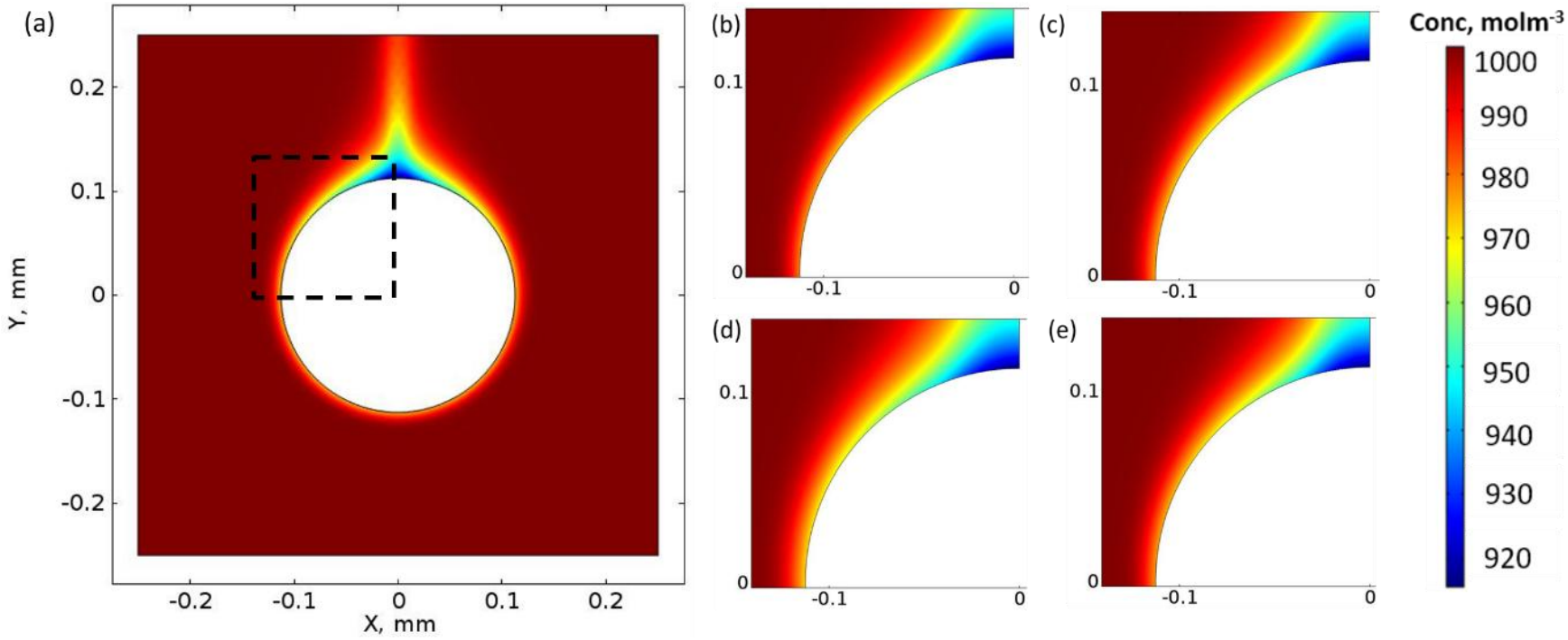
(a)
(b)
(c)
(d)
(e)
Y, mm
X, mm
0.2
0.1
0
-0.1
-0.2
Conc, molm-3
1000
990
980
970
960
950
940
930
920

Figure 7

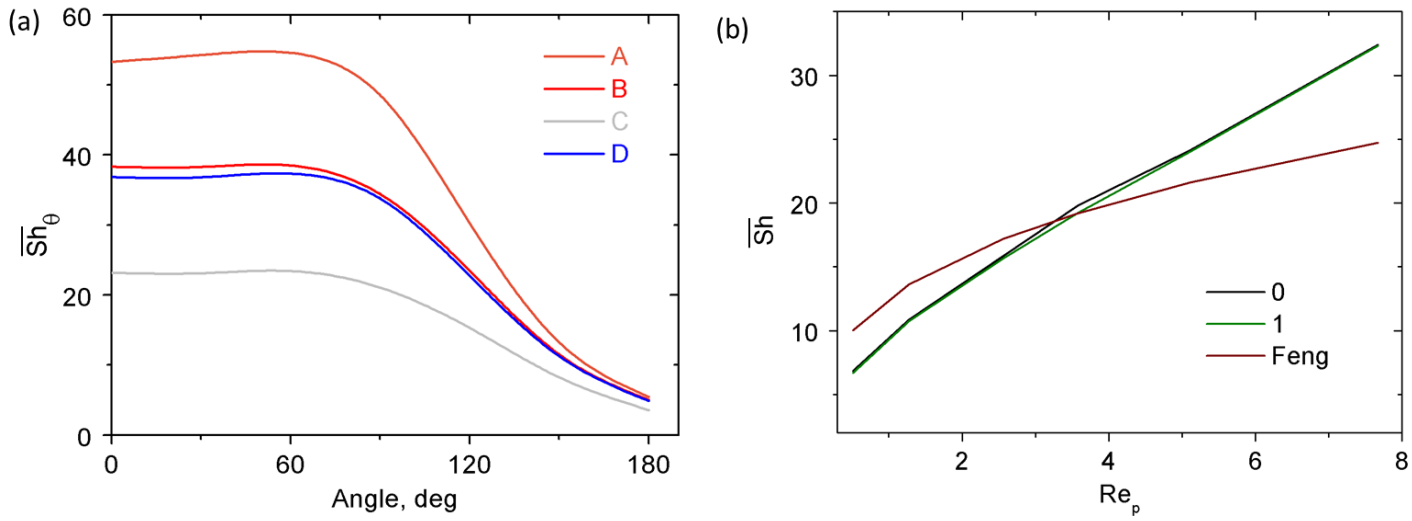
(a)
60
40
20
0
0
60
120
180
Angle, deg
$\overline{Sh}_\theta$
A
B
C
D
(b)
30
20
10
2
4
6
8
Re_p
$\overline{Sh}$
0
1
Feng

Figure 8

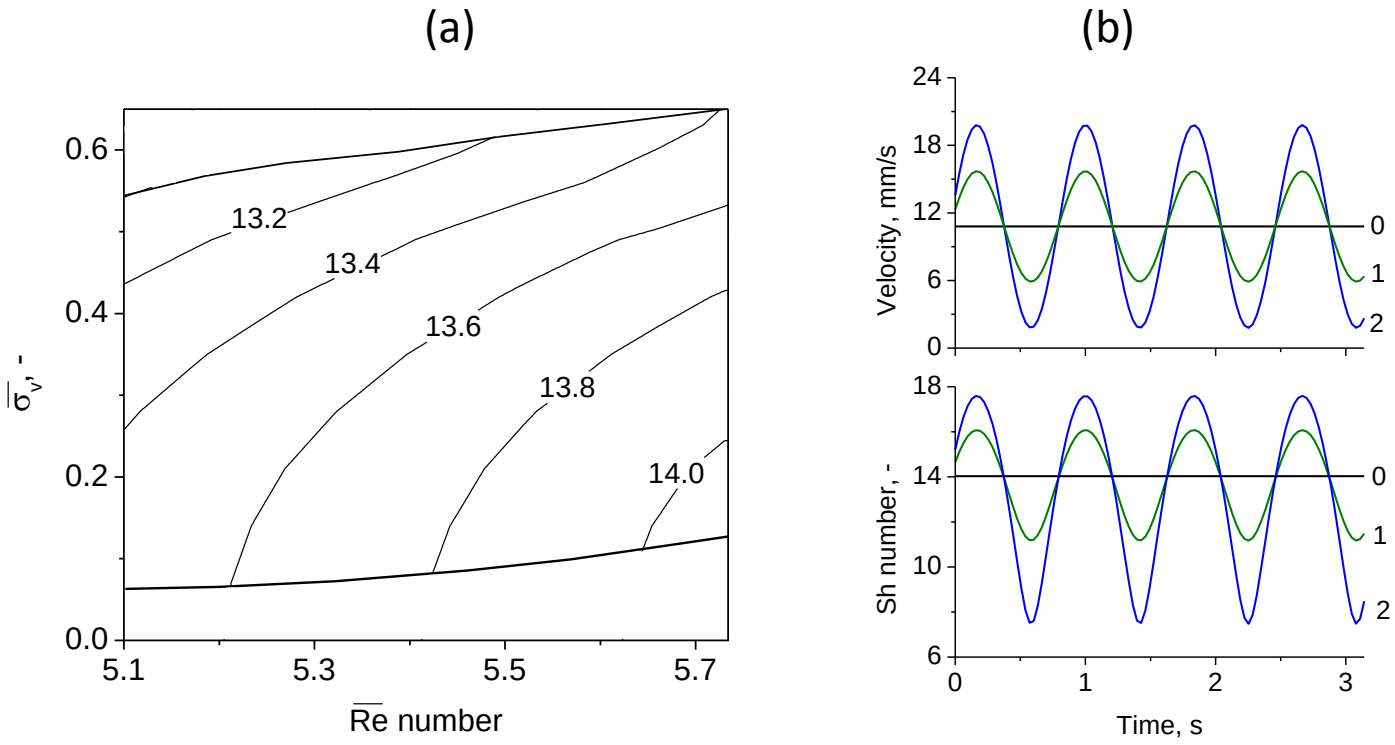
(a)
(b)
0.6
0.4
0.2
0.0
5.1
5.3
5.5
5.7
13.2
13.4
13.6
13.8
14.0
Re number
24
18
12
6
0
Velocity, mm/s
0
1
2
18
14
10
6
Sh number, -
0
1
2
3
Time, s

Figure 9

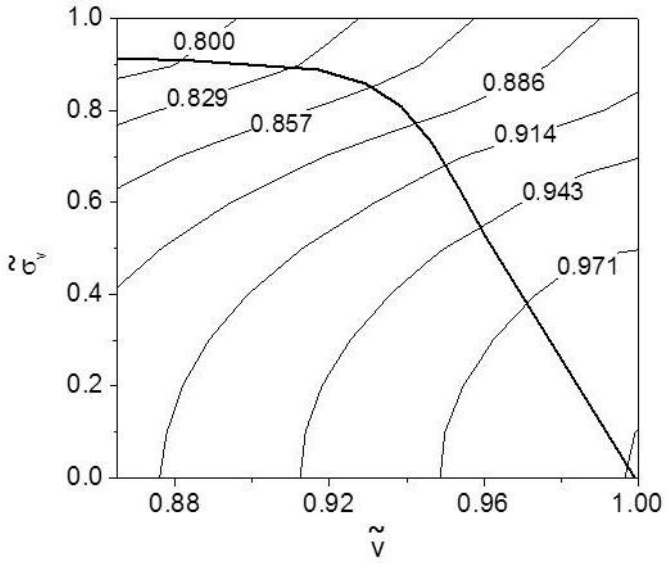
1.0
0.8
0.6
0.4
0.2
0.0
0.88
0.92
0.96
1.00
$\tilde{\sigma}_v$
$\tilde{v}$
0.800
0.829
0.857
0.886
0.914
0.943
0.971

Figure 10

(a)

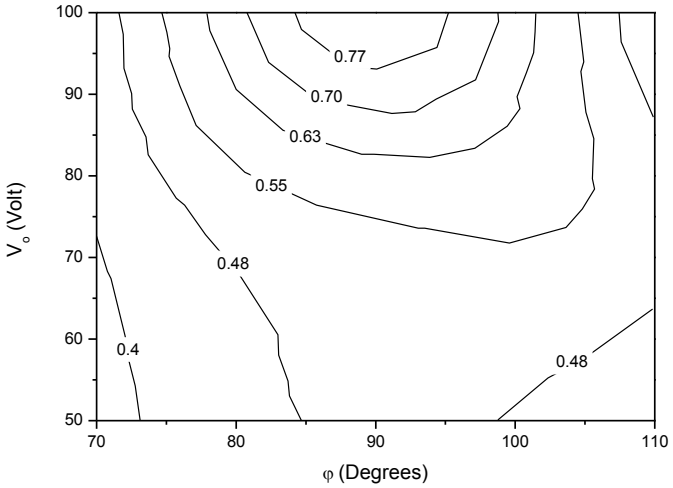
100
90
80
70
60
50
70
80
90
100
110
V_o (Volt)
φ (Degrees)
0.77
0.70
0.63
0.55
0.48
0.4
0.48

(b)

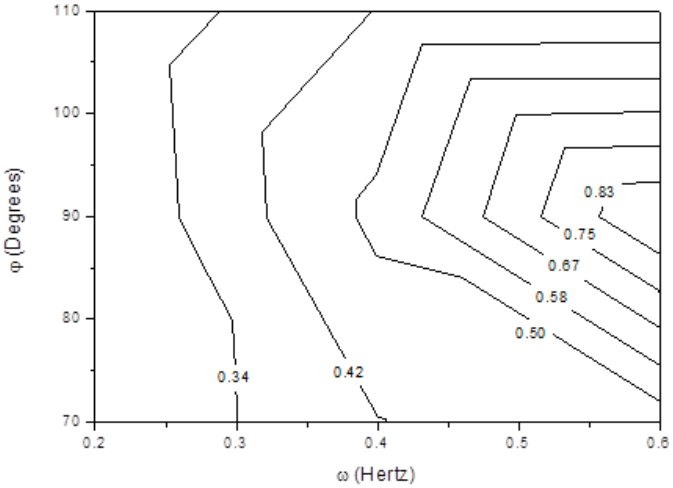
110
100
90
80
70
0.2
0.3
0.4
0.5
0.6
φ (Degrees)
ω (Hertz)
0.83
0.75
0.67
0.58
0.50
0.34
0.42

Figure 11